Bidirectional ventricular tachycardia: Ping pong in the His–Purkinje system

Alex A. Baher, MD,* Matthew Uy, BSc,* Fagen Xie, PhD,* Alan Garfinkel, PhD,*‡ Zhilin Qu, PhD,* James N. Weiss, MD*†

*From the Cardiovascular Research Laboratory, Departments of *Medicine (Cardiology), †Physiology, and ‡Integrative Biology and Physiology, David Geffen School of Medicine at UCLA, Los Angeles, California.*

BACKGROUND Bidirectional ventricular tachycardia (BVT), which is characterized by an alternating beat-to-beat ECG QRS axis, is a rare but intriguing arrhythmia associated with digitalis toxicity, familial catecholaminergic polymorphic ventricular tachycardia (CPVT), and several other conditions that predispose cardiac myocytes to delayed afterdepolarizations (DADs) and triggered activity. Evidence from human and animal studies attributes BVT to alternating ectopic foci originating from the distal His–Purkinje system in the left and/or right ventricle, respectively.

OBJECTIVE The purpose of this study was to evaluate a simple "ping pong" model of reciprocating bigeminy to explain BVT.

METHODS: We constructed a two-dimensional anatomic model of the rabbit ventricles with a simplified His–Purkinje system, in which different sites in the His–Purkinje system had different heart rate thresholds for DAD-induced bigeminy.

RESULTS When the heart rate exceeded the threshold for bigeminy at the first site in the His–Purkinje system, ventricular bigeminy developed, causing the heart rate to accelerate and exceed the threshold for bigeminy at the second site. Thus, the triggered beat from the first site induced a triggered beat from the second site. The triggered beat from the second site next reciprocated by inducing a triggered beat from the first site, and so forth. Bigeminy from two sites produced BVT, and that from three or more sites produced polymorphic VT.

CONCLUSION This "ping pong" mechanism of reciprocating bigeminy readily produces the characteristic ECG pattern of BVT and its degeneration to polymorphic VT if additional sites develop bigeminy.

KEYWORDS Action potential; Arrhythmia mechanism; Catecholaminergic polymorphic ventricular tachycardia; Electrophysiology; Ventricular tachycardia

ABBREVIATIONS **AP** = action potential; **BVT** = bidirectional ventricular tachycardia; **CPVT** = catecholaminergic polymorphic ventricular tachycardia; **DAD** = delayed afterdepolarization; **ECG** = electrocardiogram; **HPS** = His–Purkinje system; **LBB** = left bundle branch; **PVC** = premature ventricular complex; **RyR2** = ryanodine receptor; **RBB** = right bundle branch; **SR** = sarcoplasmic reticulum; **VF** = ventricular fibrillation; **VT** = ventricular tachycardia

(Heart Rhythm 2011;8:599–605)

Introduction

Bidirectional ventricular tachycardia (BVT) is characterized by beat-to beat alternation of the QRS axis on the electrocardiogram (ECG). Although uncommon, it has fascinated clinicians since its original description in 1922 as a manifestation of digitalis toxicity.[1–4] It has also been reported in the setting of hypokalemic periodic paralysis,[5] Andersen-Tawil syndrome,[6] and fulminant myocarditis.[7] More recently, BVT has also been recognized as a hallmark of catecholaminergic polymorphic ventricular tachycardia (CPVT) syndrome, a familial disorder with a high risk of sudden cardiac death during sympathetic stimulation.[8] During exercise testing, these patients typically develop premature ventricular complexes (PVCs) and sometimes ventricular bigeminy[9–11] in association with BVT, which can self-terminate or degenerate into polymorphic VT and ventricular fibrillation (VF).[8,11,12] Although the most characteristic ECG pattern of BVT is right bundle branch (RBB) block with an alternating QRS axis,[8] other patterns, such as alternating RBB and left bundle branch (LBB) block or alternating QRS axis with a narrow QRS,[13] have also been observed. Recent genetic studies have attributed familial CPVT syndromes to defects in the cardiac ryanodine receptor (RyR2) or to calsequestrin, an associated regulatory protein in the sarcoplasmic reticulum (SR), and CPVT has been recapitulated in genetically engineered mouse models incorporating the analogous RyR2 mutations.[14,15] In these mice, abnormal RyR2 regulation predisposes myocytes to delayed afterdepolarizations (DADs) and triggered activity, analogous to digitalis toxicity. A recent optical mapping

This study was supported by NIH/NHLBI Grants P01 HL078931 and R01 HL103662, and by Laubisch and Kawata Endowments. Dr. Baher's current address is Department of Medicine, Methodist Hospital, Houston, Texas 77030. **Address reprint requests and correspondence:** Dr. James N. Weiss, UCLA School of Medicine, Division of Cardiology, Room 3645 MRL Building, Los Angeles, California 90095. E-mail address: jweiss@mednet.ucla.edu. (Received September 7, 2010; accepted November 23, 2010.)

  doi:10.1016/j.hrthm.2010.11.038

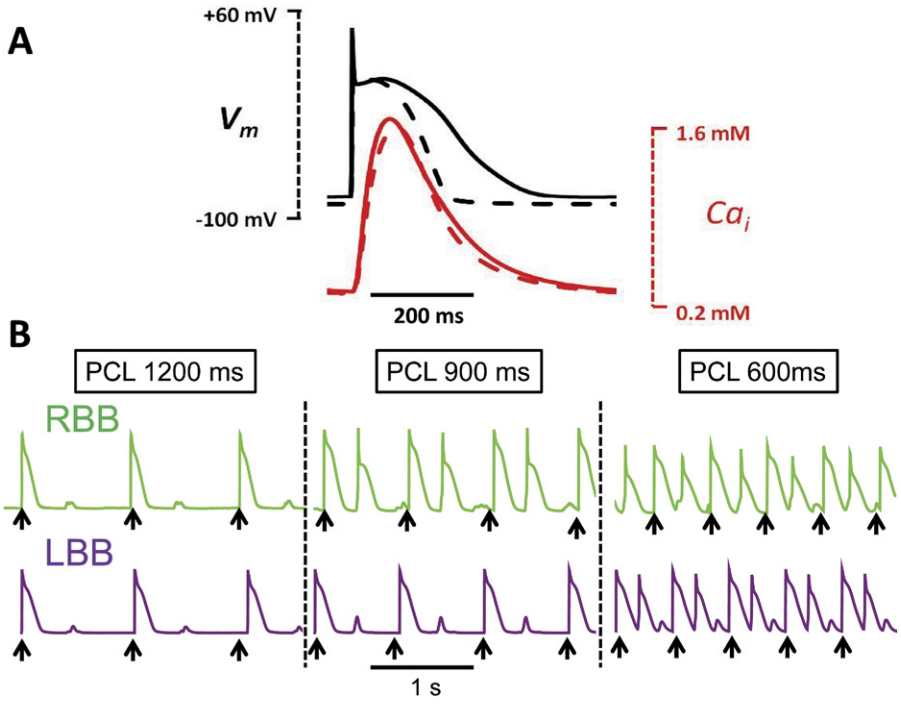

Figure 1 **A:** Comparison of simulated rabbit ventricular *(dashed line)* and Purkinje *(solid line)* action potentials (APs) and Ca_i transients during pacing at 600 ms. **B:** Rate dependence of delayed afterdepolarizations (DADs) and bigeminy in Purkinje cell AP models. For the *green trace,* the rate threshold for DAD-induced bigeminy was 67 bpm (pacing cycle length [PCL] 900 ms), such that pacing *(black arrows)* at both 900 and 600 ms induced bigeminy. For the *purple trace,* the bigeminy rate threshold was 100 bpm (PCL 600 ms), such that pacing at 600 ms, but not 900 ms, induced bigeminy. LBB = left bundle branch; RBB = right bundle branch.

study in a mouse CPVT model due to the mutation R4496C in RyR2 (RyR2-R4496C) showed that BVT was caused by two foci in the distal His–Purkinje system (HPS), one in the right ventricle and the other in the left ventricle, alternately activating the ventricles.[16] Moreover, ablation of the right ventricular HPS with Lugol solution converted BVT to monomorphic VT. These authors went on to show in a computer model of the anatomic mouse ventricles that alternate pacing from the right ventricular and left ventricular septum produced a characteristic ECG pattern of BVT. However, they did not address the mechanism by which triggered activity spontaneously generated this pattern.

Based on the observation that PVCs and ventricular bigeminy are common precursors to BVT,[9–11] it occurred to us that a simple "ping pong" mechanism, which we call *reciprocating bigeminy,* could readily account for the pattern of alternating foci observed during BVT. Although a number of mechanisms for BVT have been suggested,[10,11,17–19] the straightforward, conceptually intuitive mechanism of reciprocating bigeminy has not, to our knowledge, been explicitly proposed previously yet is fully consistent with well-known properties of triggered activity caused by DADs. We demonstrate its plausibility by incorporating these experimentally well-documented properties into computer simulations to reproduce the characteristics of BVT.

Methods

Ventricular and Purkinje action potential cell models

For ventricular cells, we used the model of Mahajan et al,[20] a detailed model of rabbit ventricular action potential (AP) that includes intracellular Ca (Ca_i) dynamics (Figure 1A, red trace). To model the Purkinje cell AP (Figure 1A, black trace), we modified $I_{to,f}$, $I_{to,s}$, I_{kr}, I_{ks}, and I_{k1} as described by Cordeiro et al.[21] We also added a background Ca current (adopted from the Luo-Rudy model[22]), using the following formulation:

$$I_{Ca,b} = \bar{G}_{Ca,b}(V - E_{Ca,b}) \quad (1)$$

$$E_{Ca,b} = \frac{RT}{2F} \ln \frac{C_O}{C_S} \quad (2)$$

where $\bar{G}_{Ca,b}$ = maximal current conductance, c_s = submembrane Ca concentration (in mM), c_o = extracellular Ca concentration (in mM), F = Faraday constant, R = universal gas constant, and T = temperature in °K. $\bar{G}_{Ca,b}$ was adjusted to produce physiologic values of diastolic and systolic Ca in the Purkinje cells and ventricular myocytes (Figure 1A and Table 1).

To produce DADs and triggered activity in Purkinje cells, we used the formulation of spontaneous SR Ca release described by Huffaker et al,[23] with some modifications. Spontaneous release was triggered solely by the SR Ca load (and not cytosolic Ca concentration), as follows:

$$J_{spon} = \bar{G}_{spon} \cdot p \cdot (c_j - c_s) \quad (3)$$

where J_{spon} = spontaneous Ca release flux, c_j = SR Ca concentration, $\bar{G}_{spon}$ = conductance of the release, and p = gating variable obeying the following equation:

Table 1 Current conductances used in Purkinje and ventricular myocyte action potential models

	Purkinje	Myocyte
$\bar{G}_{to,f}$	0.165	0.11
$\bar{G}_{to,s}$	0.06	0.04
$\bar{G}_{ca,L}$	364.0	273.0
$\bar{G}_{Ca,b}$	0.0010556	0.001508
$\bar{G}_{kr}$	0.0041625	0.0125
$\bar{G}_{ks}$	0.04615	0.1386
$\bar{G}_{k1}$	0.15	0.3
$\bar{G}_{Na}$	24.0	12.0

$$\frac{dp}{dt} = \frac{(p_\infty - p)}{\tau_p} \tag{4}$$

$$p_\infty = \begin{cases} 0 & if\ c_j < K_1 \\ \dfrac{c_j - K_1}{K_2 - K_1} & if\ K_1 < c_j < K_2 \\ 1 & if\ c_j > K_2 \end{cases} \tag{5}$$

where τ_p = 10 ms = time constant for spontaneous SR release, and K_2, K_1 = upper and lower thresholds for spontaneous SR Ca release, respectively (Table 2). With these additions, the differential equations for c_j and c_s become

$$\frac{dc_j}{dt} = -J_{rel} - J_{spon} + J_{up} + J_{leak} \tag{6}$$

$$\frac{dc_s}{dt} = \beta_s \left[\frac{\nu_i}{\nu_s}\left(J_{rel} - J_d + J_{Ca} + J_{NaCa} + J_{Ca,b} + J_{spon}\right) - J^s_{trpn} \right] \tag{7}$$

where J_{rel} = Ca-induced Ca release from the SR, J_{spon} = spontaneous release from SR due to Ca overload, J_{up} = Ca uptake by SERCA, J_{leak} = Ca leak from the SR into the cytoplasm, J_d = diffusion of Ca from the submembrane compartment (c_s) into the cytoplasmic compartment (c_i), J_{Ca} = Ca flux into the c_s from the L-type Ca channel, J_{NaCa} = flux through the Na/Ca exchanger, β_s = time-independent submembrane Ca buffering, J^s_{trpn} = time-dependent binding of Ca to troponin C, and ν_i/ν_s = cytoplasmic-to-SR volume ratio.

We also modified the equation for c_p, the effective Ca concentration sensed by the L-type Ca channel accounting for L-type Ca current inactivation due to spontaneous SR Ca release as follows:

$$\frac{dc_p}{dt} = \tilde{J}_{spon} + \tilde{J}_{SR} + \tilde{J}_{Ca} - \frac{c_p - c_s}{\tau_s} \tag{8}$$

$$\tilde{J}_{spon} = \gamma \cdot J_{spon} \tag{9}$$

where $\tilde{J}_{SR}$ and $\tilde{J}_{Ca}$ = effective fluxes from SR and Ca channel, respectively, $\tilde{J}_{spon}$ = effective flux from spontaneous SR calcium release, and γ = 200 = conversion factor.

With these modifications, the Purkinje AP model developed DADs of sufficient amplitude to cause a single triggered AP at a critical heart rate. Parameters were adjusted such that the critical heart rate at which DADs occurred could be varied (Figure 1B, green vs purple traces).

Tissue model. We used rabbit ventricular anatomy and fiber orientation data obtained from the Cardiac Mechanics Research Group at the University of California (San Diego, CA, USA), as described previously,[24,25] to extract a two-dimensional sagittal section of the ventricles (Figure 2A). We added a His–Purkinje network (with a thickness of five Purkinje cells), consisting of a His bundle dividing into an RBB and LBB, each forming further branches until inserting into the ventricular myocardium to generate a physiologic activation sequence.

Wave propagation in two-dimensional tissue was modeled using a reaction-diffusion partial differential equation:

$$\frac{\partial V_m}{\partial t} = -\frac{I_{ion}}{C_m} + \tilde{I}_{nbr} \tag{10}$$

where V_m = membrane voltage, I_{ion} = sum of the membrane currents, C_m = membrane capacitance, and $\tilde{I}_{nbr}$= diffusive flow from the neighbor cells as described below. The partial differential equations were solved using operator splitting and an adaptive time step method.[26,27] We used a variable time step between 0.001 and 0.01 ms. All simulations were performed on a 128-node Beowulf cluster.

The diffusive flow between neighboring cells was defined as follows:

$$\tilde{I}_{nbr} = D\left(\frac{V_{i+1,j}\, V_{i-1,j} - 2V_{i,j}}{dx^2}\right) + D\left(\frac{V_{i,j+1} + V_{i,j-1} - 2V_{i,j}}{dy^2}\right) \tag{11}$$

where D = 0.001 cm^2/ms if the neighboring cell was a ventricular myocyte, D = 0.006 cm^2/ms if the neighboring cell was a Purkinje cell, and dx = dy = 0.015 cm. Each cell could have up to four neighbors. Purkinje cells were coupled to ventricular myocytes at a total of 27 sites in the terminal His–Purkinje branches (where the five terminal Purkinje cells were coupled to five adjacent ventricular cells) and at a few points within the septum (where two Purkinje cells were cou-

Table 2 I_{spon} parameters for the Purkinje action potential model exhibiting delayed afterdepolarizations, located in the left bundle branch, right bundle branch, and distal Purkinje–muscle junction, as shown in Figure 2

	G_{spon}	K_1	K_2	τ_p
Right bundle branch	250.0	110.0	110.1	10.0
Left bundle branch	180.0	111.5	111.6	10.0
Purkinje–muscle junction	215.0	111.0	111.1	10.0

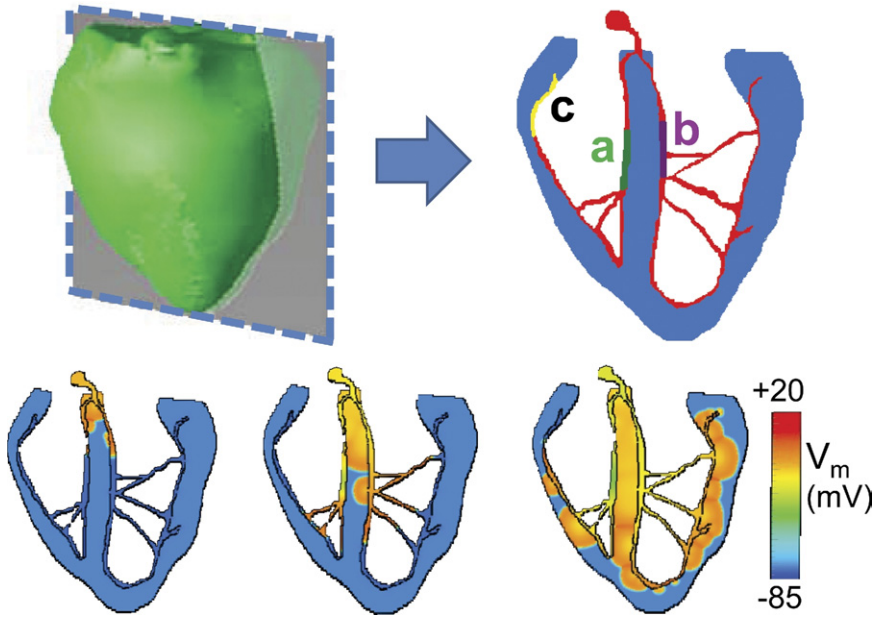

Figure 2 **A:** Anatomic rabbit ventricle model *(green)* showing a two-dimensional section *(blue)* of myocardium with the His-Purkinje system *(red)* incorporated. Regions of the His-Purkinje system susceptible to delayed afterdepolarization (DAD)-induced bigeminy in the right bundle branch *(a, green)* and left bundle branch *(b, purple)* are indicated. In some simulations, a third region *(yellow)* also developed DAD-induced bigeminy. **B:** Voltage snapshots of normal activation when the His bundle is paced.

pled to two adjacent ventricular cells). The diffusive current at Purkinje-myocyte interfaces was defined as follows:

$$\tilde{I}_{nbr} = D_p\left(\frac{V_{i+1,j} - V_{i,j}}{dx^2}\right) + D_v\left(\frac{V_{i-1,j} - V_{i,j}}{dx^2}\right) \quad (12)$$

where $D_p = 0.006$ and $D_v = 0.001$ cm^2/ms.

When the His bundle was paced (simulating a sinus beat), the resulting activation sequence is shown in Figure 2B. Activation was earliest at the left septum, followed by right septum, ventricular apex, and lateral ventricular walls, generally consistent with the ventricular activation sequence during sinus rhythm.[28,29] Within the HPS, regions of the RBB and LBB (labeled a and b, respectively) were assigned the DAD-generating Purkinje cell AP models (corresponding to the two traces in Figure 1B), with the remainder of the HPS composed of the standard Purkinje cell AP model without DADs (Figure 1A). In some simulations, a third area (labeled c) was also assigned DAD-generating Purkinje cell AP models.

Pseudo-ECG calculation. A pseudo-ECG (Φ_s) was computed from membrane voltage using the following integral expression[30]:

$$\Phi_s(x',y',z') = D\int\left[-\nabla V_m \cdot \left(\nabla\frac{1}{r}\right)\right]dx + D\int\left[-\nabla V_m \cdot \left(\nabla\frac{1}{r}\right)\right]dy \quad (13)$$

$$r = \left[(x-x')^2 + (y-y')^2 + (z-z')^2\right] \quad (14)$$

where ∇V_m = spatial gradient of V_m, and r = distance from a source point *(x,y,z)* to the location of the "electrode" at *(x',y',z')*.

Results

The proposed "ping pong" mechanism of BVT is based on the following two commonly observed behaviors of DAD-mediated triggered activity: (1) above a certain threshold heart rate, a DAD triggers a single AP after each paced AP, initiating ventricular bigeminy (Figure 1B); and (2) the threshold heart rate for bigeminy varies at different locations in the heart (Figure 1B, a and b, respectively). From the experimental evidence indicating that BVT arises from the bundle branches of the HPS,[16] we assume that the sites from which bigeminy arises are located in the HPS, where source-sink relationships are more favorable for DAD formation than in ventricular muscle.[31,32] The different heart rate thresholds for bigeminy are a natural assumption because if the rate thresholds were the same everywhere, all rate-dependent DAD-mediated PVC's arising from the HPS would have a narrow QRS complex, which is not true. We arbitrarily chose the RBB to have the lower heart rate threshold for bigeminy, set at 67 bpm, and the LBB to have the higher threshold, set at 100 bpm (Figure 3, and Movie in Online Supplement). Thus, when the heart rate exceeded 67 bpm, the paced AP with a normal activation sequence (top row) was followed by a triggered AP from the RBB, producing a QRS morphology resembling LBB block (middle row). With the onset of ventricular bigeminy, however, the average heart rate now doubled, exceeding the 100 bpm threshold for bigeminy to develop in the LBB. Thus, the triggered beat from the RBB elicited a triggered beat from

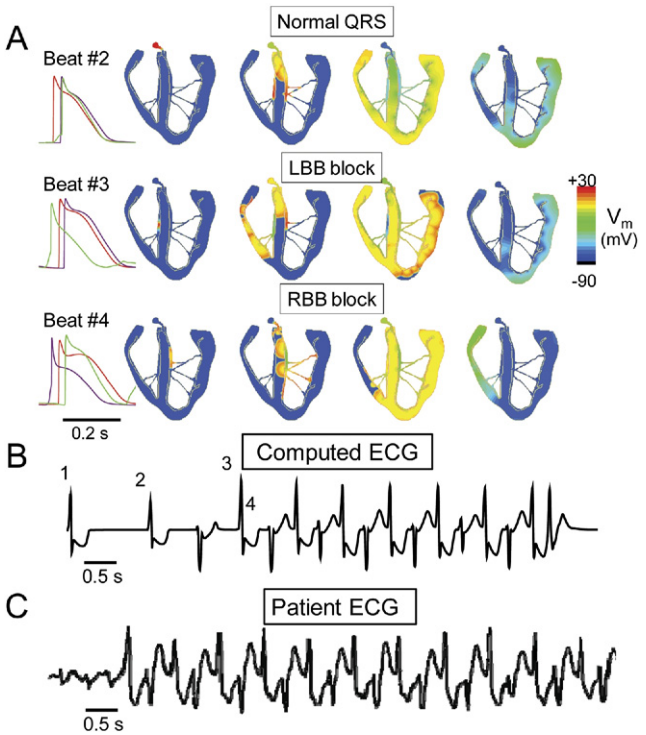

Figure 3 Simulated bidirectional ventricular tachycardia (BVT). **A:** Voltage snapshots showing the activation sequence at the onset of BVT. Beat #2 is the last paced beat, with normal activation. Beat #3 is the first beat of BVT, due to a delayed afterdepolarization (DAD)-triggered action potential (AP) arising in the right bundle branch (RBB), resulting in a QRS with a left bundle branch (LBB) block pattern. Beat #4 is the second beat of BVT, due to a DAD-triggered AP arising in the LBB, resulting in a QRS with RBB block pattern. Traces on the **right** show the timing of APs recorded from the His bundle *(red),* RBB *(green),* and LBB *(purple).* **B:** Computed ECG from the simulation in A, showing BVT. **C:** ECG recorded in a patient during BVT.[12]

the LBB, producing a QRS morphology resembling RBB block (bottom row). The arrival of this beat in the RBB then caused a triggered AP arising from the RBB, with LBB block morphology, and so forth, in a "ping pong" fashion. Figure 3B shows that the computed ECG from the model closely resembles that recorded from a patient during BVT.[12] Thus, each triggered AP from the RBB reciprocally triggers an AP from LBB, and vice versa, producing VT with an alternating LBB/RBB block pattern, as shown by the orange symbols in Figure 4. In the example shown in Figure 3, BVT terminated spontaneously, as often occurs clinically, but sustained BVT was also simulated with different parameter settings. Had we chosen the LBB to have the lower heart rate threshold for bigeminy, the results would be the same, except that the BVT would have begun with an RBB block QRS morphology instead of LBB block.

This same scenario can also account for the classic human CPVT pattern of RBB block with alternating QRS axis, assuming that the two bigeminal foci are located in distal regions of the left anterior and left posterior fascicles of the LBB (Figure 4, blue symbols). Thus, the reciprocating bigeminal beats arising from the distal left posterior and anterior fascicles would exhibit RBB block with left- and right-axis deviation, respectively. Cases of BVT have also been reported in which the axis alternates, but the QRS is narrow.[13] This variant could be explained by bigeminal beats arising alternately from the anterior and posterior fascicles but conducting retrogradely and blocking anterogradely (Figure 4, brown symbols). Thus, retrograde conduction to the contralateral fascicle and RBB would result in a narrow QRS with right- or left-axis deviation.

Finally, we simulated the degeneration of BVT into polymorphic VT by assuming that when BVT further increases heart rate, additional sites in the HPS are recruited to develop bigeminy. Figure 5 shows a scenario where an additional site exists at a Purkinje–myocyte junction in the right ventricular free wall. When this third site developed triggered ventricular bigeminy, the earliest activation occurred irregularly among the three sites, creating a polymorphic VT pattern on the computed ECG, similar to that observed in a patient.[12] Similar patterns developed when more than three sites develop spontaneous SR Ca release activity (data not shown).

Discussion

Both supraventricular or ventricular mechanisms of BVT involving either focal or reentrant mechanisms have been proposed.[10] A supraventricular mechanism with alternating left anterior and left posterior fascicular block[17] was largely excluded with the advent of intracardiac recordings, which failed to show a His-bundle potential preceding the alternating QRS complexes during BVT.[18,19] Postulated ventricular mechanisms have included a single focus in the proximal His bundle or bundle branches with alternating left fascicular block, or single or double foci in the distal HPS. In the single focus case, there is no obvious explanation for why fascicular or bundle branch block should alternate during BVT. Usually, concealed retrograde conduction per-

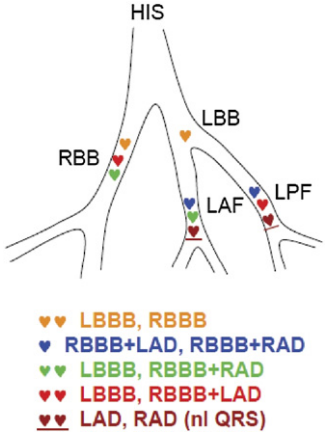

Figure 4 ECG patterns of bidirectional ventricular tachycardia corresponding to locations of pairs of foci with reciprocating bigeminy. See text for details. HIS = His bundle; LAD = left-axis deviation; LAF = left anterior fascicle; LBB = left bundle branch; LBBB = left bundle branch block; LPF = left posterior fascicle; RAD = right-axis deviation; RBB = right bundle branch; RBBB = right bundle branch block.

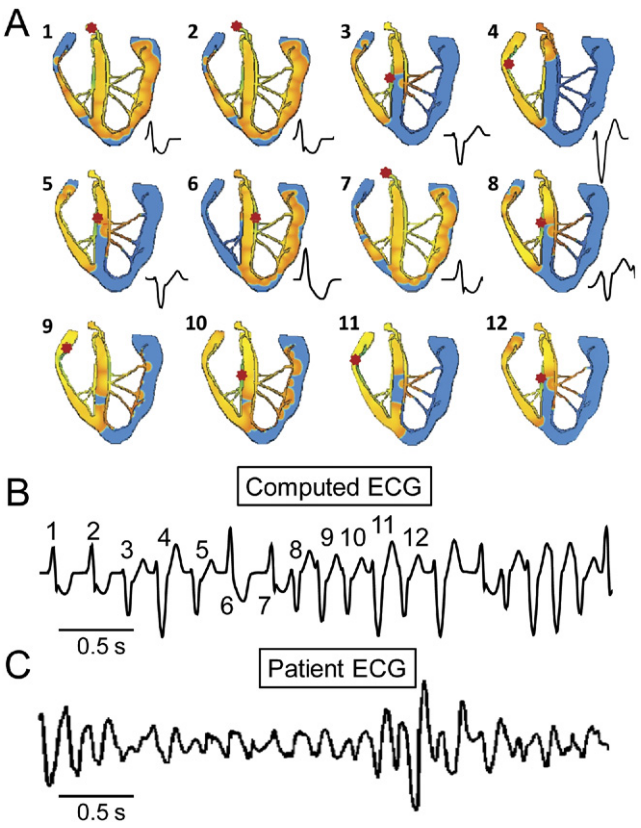

Figure 5 Simulated polymorphic ventricular tachycardia (VT). **A:** Voltage snapshots showing the activation sequences corresponding to different QRS morphologies during polymorphic VT caused by three foci with reciprocating bigeminy. *Red dot* in each panel indicates the earliest activation site. **B:** Computed ECG from the simulation in A, showing polymorphic VT (with beat numbers corresponding to snapshots in A). **C:** ECG recorded from a patient with catecholaminergic polymorphic VT.[12]

petuates block in the fascicle/bundle branch that initially develops conduction block. Even if a conduction gap prevents concealed retrograde conduction from perpetuating block, both fascicles/bundle branches would have to exhibit the same conduction gap phenomena, which seems highly unlikely. In the double foci case, if neither focus is protected by entrance block, the faster focus should overdrive the slower focus, producing monomorphic VT rather than BVT. If both foci are protected by entrance block, then they would need to have identical cycle lengths, phase shifted by exactly 180° to produce a constant cycle length during BVT, which also is improbable. If only one focus is protected by entrance block, then it could induce a second focus to fire at a fixed coupling interval, but the coupling interval would have to be exactly half of the first focus's cycle length to produce a constant cycle length during BVT.

In contrast to these complicated mechanisms, reciprocating bigeminy solves the puzzle of alternating QRS morphology by a simple "ping pong" mechanism in which DAD-induced triggered activity develops at different heart rate thresholds in different regions of the HPS or ventricles, consistent with known cellular properties of DAD-induced triggered activity.[28,33,34] To produce a constant (i.e., nonalternating) cycle length during BVT requires only that the coupling intervals of the triggered beats be similar at the two sites.

Although we have modeled the bigeminy to be due to triggered activity from DADs, the same results are predicted for any mechanism inducing ventricular bigeminy (including automaticity or reentry) at more than one location in the ventricles. In addition, there is no strict requirement for the two bigeminal foci to be located in the distal HPS in opposite fascicles or ventricles. For example, two reciprocating triggered foci located in the same ventricle,[8] or at sites in the endocardium and epicardium, could also produce BVT by this mechanism,[35] although the QRS axis and morphology changes would be different. However, in humans, the most common BVT pattern during digitalis toxicity and CPVT is RBB block with alternating right- and left-axis deviation, consistent with reciprocating ectopic foci located in the distal left anterior and posterior fascicles of the left bundle. In mice, due to their smaller heart size, the more common pattern may be foci located on opposite sides of the interventricular septum.

Finally, we show that if the increased heart rate during BVT induces a third bigeminal focus in the HPS, the interactions among the three foci can produce irregular activation patterns resulting in polymorphic VT (Figure 5). Because the model is deterministic, the irregularity may be due to chaos, which is a common scenario observed with coupled oscillators.[36] As heart rate progressively accelerates, we speculate that additional regions develop DADs, making the conversion to VF progressively more likely.

In summary, we conjecture that the full spectrum of arrhythmias described electrocardiographically in acquired and familial conditions associated with BVT can be accounted for based on the known properties of DAD-triggered arrhythmias, as follows:

Ventricular bigeminy, when a single site in the HPS or ventricular myocardium develops a single DAD-triggered beat following each sinus beat.

BVT, when a second site develops ventricular bigeminy and reciprocally activates the first site by the ping pong mechanism described.

Polymorphic VT, when three or more sites concurrently develop bigeminy. Note that these first three mechanisms specifically require bigeminy, that is, DADs are capable of triggering only a single PVC following each sinus or paced beat so that the subsequent beat has to arise from a different location (thereby altering QRS morphology/axis).

Monomorphic VT, when bigeminy progresses to repetitive DADs, which generate a run of triggered activity such that the site with the most rapid rate of triggered activity overdrives the other slower sites, producing a monomorphic QRS complex.

Degeneration to VF, when any of these VT forms results in wavebreak and initiation of reentry, which is then likely

to be maintained by a mixture of reentry and DAD-triggered focal activations.

Study limitations

Several limitations of our study should be recognized. Our Purkinje AP model is an approximation that does not replicate all experimental details, such as a lowered AP plateau.[21] We did not attempt to build a complete "bottom up" model linking Ca waves and DADs at the subcellular–cellular levels to DADs and triggered activity at the tissue–whole heart levels. In particular, Ca waves and DADs at the cellular level are strongly influenced by stochastic factors. How they overcome source-sink mismatches in well-coupled tissue to produce regular behaviors such as ventricular bigeminy is not well understood. Nevertheless, periodic arrhythmias attributed to DADs, such as ventricular bigeminy, are commonly observed in cardiac tissue[28,33,34] in the setting of glycoside toxicity and in association with BVT.[9–11] The experimental observation that PVCs with wide QRS complexes arise from the HPS during or after rapid pacing also implies that different regions of the heart must have different rate thresholds for DAD-mediated triggered activity; otherwise, PVCs all would have a narrow QRS complex. This is not surprising because many factors influence the precise rate threshold at which DADs cause triggered activity, including cell properties, intercellular coupling, geometric factors influencing the source-sink relationship in the bundle branches and HPS, etc. To illustrate the general feasibility of the reciprocating bigeminy mechanism, we phenomenologically introduced these well-documented experimental features into our computer model, rather than building a highly detailed model from the bottom up incorporating stochastic elements, etc. To simplify computer modeling, we also simulated a ventricular slice rather than the full three-dimensional anatomic heart. However, this is not likely to change the findings because the ventricular myocardium simply acts as a passive electrical conduit for the ping pong dynamics occurring in the HPS.

Acknowledgment

We thank Tannaz Tebbi for technical assistance.

Appendix

Supplementary data

Supplementary data associated with this article can be found, in the online version, at doi:10.1016/j.hrthm.2010.11.038.

References

1. Schwensen C. Ventricular tachycardia as the result of the administration of digitalis. Heart 1922;9:199–204.
2. Valent S, Kelly P. Digoxin-induced bidirectional ventricular tachycardia. N Engl J Med 1997;336:550.
3. Kummer JL, Nair R, Krishnan SC. Bidirectional ventricular tachycardia caused by digitalis toxicity. Circulation 2006;113:e156–e157.
4. Menduiña MJ, Candel JM, Alaminos P, et al. Bidirectional ventricular tachycardia due to digitalis poisoning. Rev Esp Cardiol 2005;58:991–993.
5. Stubbs WA. Bidirectional ventricular tachycardia in familial hypokalaemic periodic paralysis. Proc R Soc Med 1976;69:223–224.
6. Morita H, Zipes DP, Morita ST, et al. Mechanism of U wave and polymorphic ventricular tachycardia in a canine tissue model of Andersen-Tawil syndrome. Cardiovasc Res 2007;75:510–518.
7. Berte B, Eyskens B, Meyfroidt G, et al. Bidirectional ventricular tachycardia in fulminant myocarditis. Europace 2008;10:767–768.
8. Leenhardt A, Lucet V, Denjoy I, et al. Catecholaminergic polymorphic ventricular tachycardia in children : a 7-year follow-up of 21 patients. Circulation 1995;91:1512–1519.
9. Levy S, Hilaire J, Clementy J, et al. Bidirectional tachycardia. Mechanism derived from intracardiac recordings and programmed electrical stimulation. Pacing Clin Electrophysiol 1982;5:633–638.
10. Levy S, Aliot E. Bidirectional tachycardia: a new look on the mechanism. Pacing Clin Electrophysiol 1989;12:827–834.
11. Sumitomo N, Harada K, Nagashima M, et al. Catecholaminergic polymorphic ventricular tachycardia: electrocardiographic characteristics and optimal therapeutic strategies to prevent sudden death. Heart 2003;89:66–70.
12. Lin YH, Lai LP, Lin TK, et al. Exercise-provoked bidirectional ventricular tachycardia in a young woman. J Formos Med Assoc 2004;103:780–783.
13. Rothfeld EL. Bidirectional tachycardia with normal QRS duration. Am Heart J 1976;92:231–233.
14. Cerrone M, Colombi B, Santoro M, et al. Bidirectional ventricular tachycardia and fibrillation elicited in a knock-in mouse model carrier of a mutation in the cardiac ryanodine receptor. Circ Res 2005;96:e77–e82.
15. Knollmann B, Chopra N, Hlaing T, et al. Casq2 deletion causes sarcoplasmic reticulum volume increase, premature Ca release, and catecholaminergic polymorphic ventricular tachycardia. J Clin Invest 2006;116:2510–2520.
16. Cerrone M, Noujaim SF, Tolkacheva EG, et al. Arrhythmogenic mechanisms in a mouse model of catecholaminergic polymorphic ventricular tachycardia. Circ Res 2007;101:1039–1048.
17. Rosenbaum MB, Elizari MV, Lazzari JO. The mechanism of bidirectional tachycardia. Am Heart J 1969;78:2–4.
18. Cohen SI, Deisseroth A, Hecht HS. Infra-His bundle origin of bidirectional tachycardia. Circulation 1973;47:1260–266.
19. Morris SN, Zipes DP. His bundle electrocardiography during bidirectional tachycardia. Circulation 1973;48:32–6.
20. Mahajan A, Shiferaw Y, Sato D, et al. A rabbit ventricular action potential model replicating cardiac dynamics at rapid heart rates. Biophys J 2008;94:392–10.
21. Cordeiro JM, Spitzer KW, Giles WR. Repolarizing K currents in rabbit heart Purkinje cells. J Physiol 1998;508:811–23.
22. Luo CH, Rudy Y. A dynamic model of the cardiac ventricular action potential. 1. Simulations of ionic currents and concentration changes. Circ Res 1994;74:1071–1096.
23. Huffaker RB, Samade R, Weiss JN, et al. Tachycardia-induced early afterdepolarizations: insights into potential ionic mechanisms from computer simulations. Comput Biol Med 2008;38:1140–1151.
24. Xie F, Qu Z, Yang J, Baher A, et al. A simulation study of the effects of cardiac anatomy in ventricular fibrillation. J Clin Invest 2004;113:686–693.
25. Baher A, Qu Z, Hayatdavoudi A, et al. Short-term cardiac memory and mother rotor fibrillation. Am J Physiol Heart Circ Physiol 2007;292:H180–H189.
26. Qu Z, Garfinkel A. An advanced algorithm for solving partial differential equation in cardiac conduction. IEEE Trans Biomed Eng 1999;46:1166–1168.
27. Qu Z, Weiss JN, Garfinkel A. Cardiac electrical restitution properties and stability of reentrant spiral waves: a simulation study. Am J Physiol 1999;45: H269–H283.
28. Braunwald E. Heart Disease: A Textbook of Cardiovascular Medicine. Philadelphia: WB Saunders, 1980.
29. Azarov JE, Shmakov DN, Vityazev VA, et al. Activation and repolarization patterns in the ventricular epicardium under sinus rhythm in frog and rabbit hearts. Comp Biochem Physiol A Mol Integr Physiol 2007;146:310–316.
30. Gima K, Rudy Y. Ionic current basis of electrocardiographic waveforms: a model study. Circ Res 2002;90:889–896.
31. Maruyama M, Joung B, Tang L, et al. Diastolic intracellular calcium-membrane voltage coupling gain and postshock arrhythmias: role of Purkinje fibers and triggered activity. Circ Res 2010;106:399–408.
32. Xie Y, Sato D, Garfinkel A, Qu Z, et al. So little source, so much sink: requirements for afterdepolarizations to propagate in tissue. Biophys J 2010;99: 1408–1415.
33. Ferrier GR, Saunders JH, Mendez C. A cellular mechanism for the generation of ventricular arrhythmias by acetylstrophanthidin. Circ Res 1973;32:600–609.
34. Garfinkel A, Spano ML, Ditto WL, et al. Controlling cardiac chaos. Science 1992;257:1230–1235.
35. Nam GB, Burashnikov A, Antzelevitch C. Cellular mechanisms underlying the development of catecholaminergic ventricular tachycardia. Circulation 2005; 111:2727–2733.
36. Hilborn RC. Chaos and Nonlinear Dynamics. Volume 6. New York: Oxford University Press, 1994.